






Robust and efficient EBG-backed wearable antenna for ISM applications

Ayesha Saeed¹ , Asma Ejaz^{1,*} , Humayun Shahid¹ ,
Yasar Amin^{1,2} , Hannu Tenhunen^{2,3} 

¹ACTSENA Research Group, Department of Telecommunication Engineering,
University of Engineering and Technology, Taxila, Pakistan

²Department of Electronic Systems, Royal Institute of Technology (KTH), Stockholm, Sweden

³Department of Information Technology, TUCS, University of Turku, Turku, Finland

Received: 13.01.2021

Accepted/Published Online: 16.09.2021

Final Version: 30.11.2021

Abstract: A structurally compact, semiflexible wearable antenna composed of a distinctively miniaturized electromagnetic band gap (EBG) structure is presented in this work. Designed for body-centric applications in the 5.8 GHz band, the design draws heavily from a novel planar geometry realized on Rogers RT/duroid 5880 laminate with a compact physical footprint spanning lateral dimensions of $0.6 \lambda_0 \times 0.06 \lambda_0$. Incorporating a 2×2 EBG structure at the rear of the proposed design ensures sufficient isolation between the body and the antenna, doing away with the performance degradation associated with high permittivity of the tissue layer. The peculiar antenna geometry allows for reduced backward radiation and low specific absorption rate (SAR). With the inclusion of EBG, the gain of the antenna undergoes a considerable increase to 7.2 dBi with more than 95% reduction in SAR value. In addition, the front-to-back ratio also amplified to 13 dB. A rigorous analysis detailing the structural robustness is reported for varied bend angle configurations of the proposed antenna. To assess the suitability of the proposed design as a body-worn antenna, an experimental investigation is carried out on different parts of the body. Experimental findings are congruent with computationally obtained results, validating the applicability of the novel antenna structure for body-worn applications.

Key words: Wearable antenna, artificial ground plane, electromagnetic bandgap (EBG), specific absorption rate (SAR)

1. Introduction

Wearable antenna, which was once an envisioned thought in the pragmatic world of wireless technology has lately opened a new paradigm of endless possibilities in our everyday living with its diverse applications in health care, military, and navigation [1, 2].

In the context of body-centric communication [3], antenna plays a significant role in facilitating a reliable link between the human body and the device, which thereby, elicits us to design compact antennas that are light-weight and low profile to facilitate easy integration. Additionally, bearing in mind the wearer's comfort, the antennas are mandated to be flexible and mechanically robust to a suitable extent to cater for the dynamics of human body [4]. Besides flexibility, one of the major considerations in designing an efficient wearable antenna is its on-body performance and the challenges that come along. A consequence of placing an electronic device in the vicinity of a human subject is emergence of detrimental effects of the body that hamper the overall performance, mainly due to the high permittivity and dispersive nature of biological tissues. The EM radiations emitted by the antenna are thus absorbed by the human body, quantified by specific absorption rate (SAR),

*Correspondence: asma.ejaz@uettaxila.edu.pk

leaving a derogatory impact on the antenna performance in terms of drastically altered radiation properties and impedance mismatch [5, 6].

In literature, considerable number of antenna designs [7, 8] have been analyzed for their usefulness and suitability in the body-worn configuration including patch antenna [9, 10], planar inverted F (PIFA) [11] and planar monopoles [12]. However, most of the reported antennas are either constricted by complex geometry or have a large lateral size with a narrow bandwidth (BW). On the other hand, CPW-fed antennas are a preferred choice for designing wearables with its ground located on either side of the feed and positioned over the dielectric, provides simple configuration and several fabrication advantages over other reported antennas [13, 14].

Wearable antennas, as the name suggests, need to be conformal and flexible. Thereof, to account for the structural deformation when bent in case of flexible antennas [15], several textile and nontextile [18] antennas have been proposed in literature with the most common choices being jeans/denim [19], felt [17], Kapton polyimide [20] and polydimethylsiloxane PDMS substrate [16] exhibiting enhanced features like flexibility, compatibility of integration into clothes and improved overall performance. However, fabric substrates cannot sustain environmental effects and the dynamics of body movement, and thereof conditionally crumple; thus, stable performance is not guaranteed. Also, the relatively higher cost of specialized substrates, limited commercial availability and rather difficult fabrication process reinforces us to employ low cost, readily available substrates in designing antennas for wearable purposes [5].

Extracts from the present-day literature include research by Hamouda et al. [20], in which a flexible polymer-based monopole wearable antenna was presented. The design was relatively simple and featured good corrosion resistance and low weight, but its large footprint and high backward radiation limits its utility in wearables. In the research by Arif et al. [5], a compact, fractal antenna based on Koch's design technique which incorporates meandering slits to reduce size was employed. The results were satisfactory with significant size reduction at the cost of complex geometry and acceptable efficiency with high SAR levels. So far, many studies have been proposed, specifically in the study by Ashyap et al. [13], a CPW-fed C-shaped antenna integrated with EBG-FSS was investigated. The designed antenna employed denim as its substrate, seemingly flexible but of course would crumple under the undeniable effects of body movement and changing environment while its size still serving as a major constraint considering the user's comfort. Moreover, in research by El Atrash et al. [3], a triangular slotted wearable antenna backed by an AMC was analyzed and evaluated where the integration of AMC with the antenna resulted in high gain but larger dimensions.

Metamaterial usually referred to as an engineered material is constructed by periodically arranging the already available materials in such a way that it exhibits electromagnetic properties uncommon to any other found in nature [21]. Studies show that the inclusion of a metamaterial significantly improves the performance metrics of an antenna [22]. Lately, this artificially fabricated material has attracted the interest of the researchers because of the appealing properties it offers. In particular, the electromagnetic bandgap (EBG) structures [23] and the artificial magnetic conductors (AMCs) [24, 28] are classified under the broad term of metamaterials. EBG being its subset has gained considerable attention because of its ability to prevent EM wave propagation in specified direction or frequency for all of its incident or polarization states. While in the bandgap regime, their high surface impedance property can be used to enhance radiation performance in terms of gain and reduced side lobes making them a good candidate for wearable applications where reduced SAR is an ultimate requirement. Moreover, EBG exhibits in-phase reflection property which ultimately leads to good antenna efficiency because

of its ability to provide constructive image current within specified frequency bands [25].

The inclusion of EBG surface in the antenna design effectuates higher gain by suppressing the back radiation which is attained by retaining same direction for both image and original current. This property ultimately reinforces a more directional pattern. Moreover, the reduced back radiation brings about improvement in FBR, in turn repressing the SAR value which serves as the prime objective of designed wearables [3, 22]. To back the concept, several EBG design configurations have been proposed in recent literature [26] in an attempt to improve gain and maintain decent isolation amid antenna and body extending it further to reduce the SAR for a particular device.

In this paper, a conformal, robust and compact antenna integrated with a simple yet novel EBG structure is presented and verified experimentally for 5.8 GHz ISM band. The design is not only user-oriented but also practically feasible. The overall dimensions being $32 \times 32 \times 3.5 \text{ mm}^3$, demonstrate clear size reduction in comparison to the reported designs in literature [3, 6, 28] and [29]. The incorporated substrate can withstand bending without undergoing variation in its electrical properties which solidify its utility in wearables. The proposed design additionally provides high gain and reduced SAR through the embodiment of EBG, which is acting as a backing shield for antenna [27]. All the required simulations are carried out using the commercial three-dimensional (3-D) electromagnetic solver (CST Microwave Studio) [34].

2. Antenna and EBG design

2.1. Antenna design

For an antenna to be appropriate for wearable utilization, it requires design compactness to suit the targeted application area. Considering the specifications, a low-profile flexible antenna is designed within the compact dimensions of $20 \times 20 \text{ mm}^2$ ($0.38 \lambda_0 \times 0.38 \lambda_0$) for telemedicine applications. The proposed antenna intends to facilitate remote patient monitoring via a noninvasive wearable device. This is done by establishing a continual connection between the patient and care facility outside the clinical setting to proactively reach out to patients by gathering stats about their well-being in terms of diabetic level, blood pressure, etc.

Figure 1a shows the geometrical illustration of the antenna structure, which utilizes a fully planar configuration while Figure 1b presents its 3D view. The design is realized on 0.508 mm thick polymer-based dielectric substrate Rogers RT/duroid 5880 ($\epsilon_r = 2.2$ and $\delta = 0.0009$), while the radiating element features various asymmetrical slots etched on top of it. This radiating element is incised on 35 μm thick copper (cladding) with an estimated conductivity of $5.96 \times 10^7 \text{ S/m}$ [5].

A coplanar waveguide with the characteristic impedance of 50 ohms is used to excite the antenna [17]. Of the main reasons for employing a CPW feedline mechanism is the positioning of the radiating element and the ground on the same side of the substrate, which reduces much of the fabrication complexity [14].

As affirmed in [7], the insertion of slots reduces the antenna profile significantly as it diverts the current distribution, which consequently increases the current path. Hence, as manifested in stages 1 and 2, a C-shape is incised in the primarily designed microstrip square patch. The C-shaped resonator is further meandered to achieve compactness in design as demonstrated in the next stages. The asymmetric extensions, as they form the main radiator, are categorized as *e-1* and *e-2*, respectively. The meandered arm (*e-1*) is added horizontally along the radiator to lengthen the current path, which thereby, leads to a reduction in resonant frequency. The *e-2* is the vertical arm symmetric to the feedline. In general, the arms *e-1* and *e-2* conjointly control the resonance, while the gap between *e-1* and *e-2* affects the impedance match.

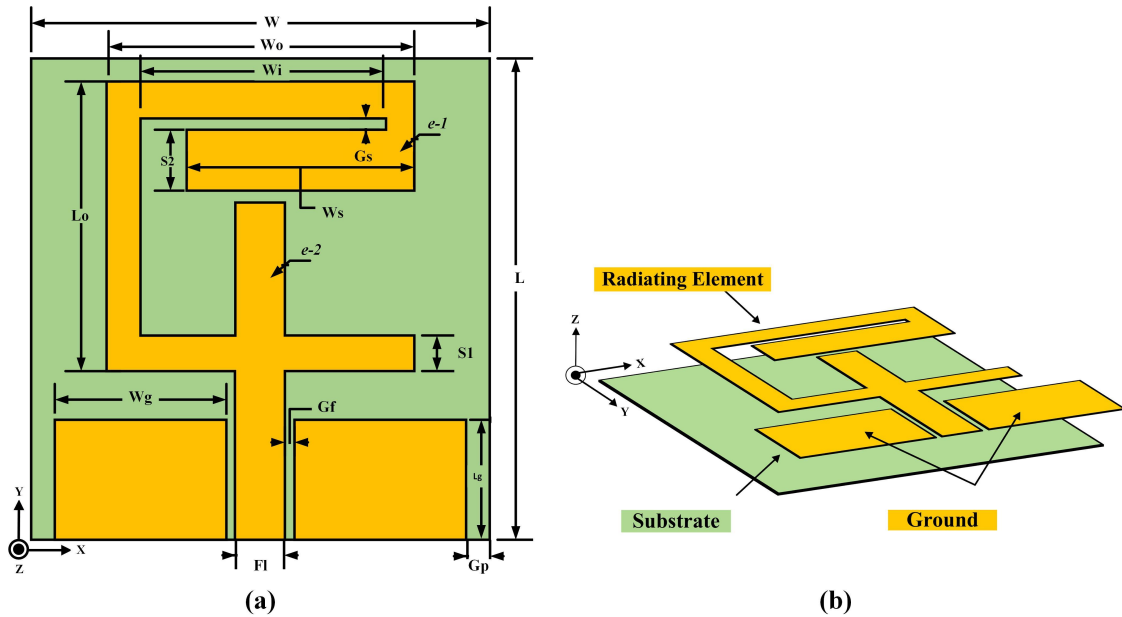


Figure 1. (a) Geometrical illustration of the proposed design with dimensions listed as $W = 20$ mm, $L = 20$ mm, $W_o = 13.40$ mm, $L_o = 12$ mm, $L_g = 5$ mm, $W_g = 7.5$ mm, $W_i = 10.7$ mm, $W_s = 9.7$ mm, $F_l = 1.16$ mm, $G_p = 1$ mm, $G_f = 1$ mm, $G_s = 0.5$ mm, $S_1 = 1.5$ mm and $S_2 = 2.5$ mm. (b) 3D illustration of the proposed design.

The overall functionality of arbitrarily shaped radiator is controlled by a set of parameters of which the W_s , defined as the length of the arm $e-1$, plays a determining role. Radiating elements outlined by various geometric parameters provide considerable freedom for tuning the design for particular frequencies. So, the dimension of W_s is carefully chosen by performing parametric analysis to avoid any discrepancies. As evident from the Figure 2, an increase in the length of the arm $e-1$ shifts the resonance to the desired frequency of operation.

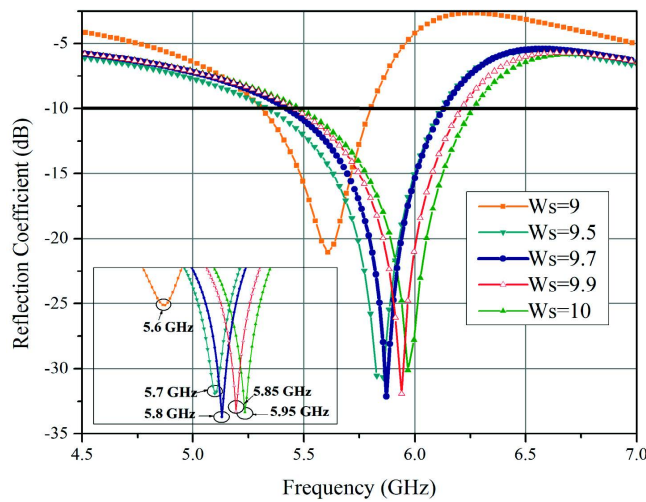


Figure 2. Parametric analysis on the W_s dimension.

2.2. EBG structure

The structural representation of the EBG unit cell is depicted in Figures 3a and 3b, respectively. Instead of the conventional mushroom-shaped EBG, a circular patch via-less configuration is utilized to reduce the design complexity that comes along with the former one.

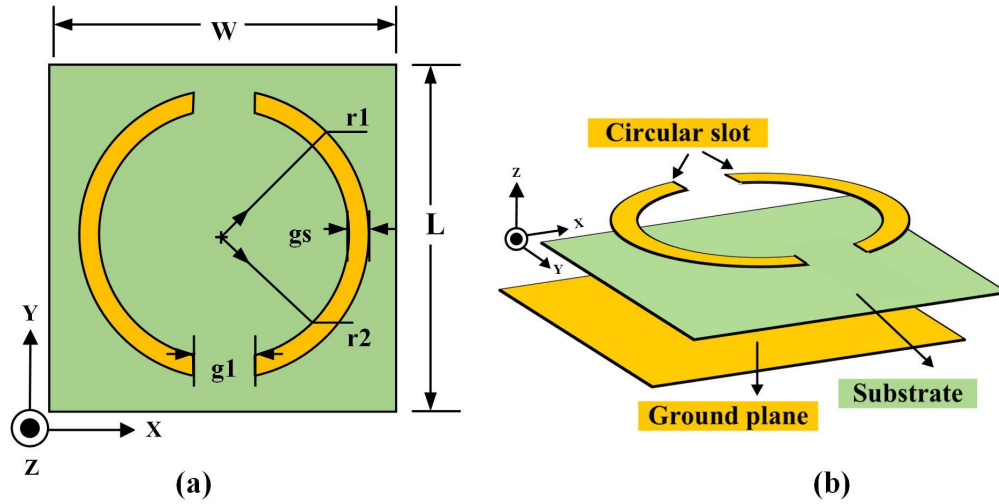


Figure 3. (a) Structural representation of the EBG unit cell with dimensions listed as $L = 16$ mm, $W = 16$ mm, $r1 = 7$ mm, $r2 = 6$ mm, $gs = 1$ mm, $g1 = 3.2$ mm. (b) 3D illustration of the proposed unit cell.

Initially, a circular patch with radius $r1$ is constructed on top of the grounded dielectric substrate which is then modified to two arc-shaped slots positioned symmetrically with reference to the centre of the patch. The substrate utilized for the EBG is the same as used for the antenna that is Rogers RT/duroid 5880. The size of the unit cell is confined to compact dimensions of $16 \times 16 \text{ mm}^2$ ($0.3\lambda_0 \times 0.3\lambda_0$) which ultimately makes the overall size for a 2×2 array to be $32 \times 32 \text{ mm}^2$ ($0.6\lambda_0 \times 0.6\lambda_0$) which is significantly low in profile than previously reported antennas [17, 28].

The resonant frequency for the periodic structure is calculated using (1) where L and C is the inductance and capacitance of the EBG surface, respectively. In general, the value of inductance and capacitance depends on the EBG geometry where L is characterized by the thickness of the substrate and C is specified by the gap among the patches [25].

$$f = \frac{1}{2\pi\sqrt{LC}} \tag{1}$$

Figure 4 shows the step by step design evolution of the proposed unit cell along with its corresponding reflection phase. The simplified design approach gives a clear picture of how the addition of symmetrical slotted arcs control the resonance frequency for a particular band [17].

For the primarily circular patch of $20 \times 20 \text{ mm}^2$ ($0.38\lambda_0 \times 0.38\lambda_0$), the resonance was around the desired frequency but at the cost of large lateral unit size. As the aim was to reduce the overall footprint, the shape was remodified to a total size of $16 \times 16 \text{ mm}^2$ ($0.3\lambda_0 \times 0.3\lambda_0$), eventually forming a circular ring. Yet the results needed enhancement, so a slot was cut in the annular ring to make the resonance fall into the desired band of operation while the thickness of arcs control the bandwidth.

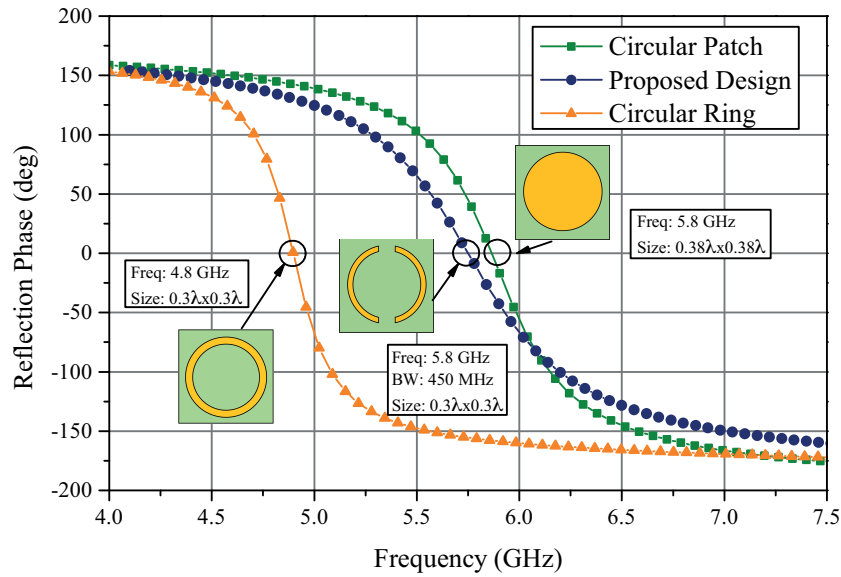


Figure 4. Design evolution of the proposed unit cell.

A parametric analysis, as shown in Figures 5a and 5b is also performed. The analysis delineates a precise study on the control mechanism of operating frequency and the bandwidth denoted by $g1$ (slotted-gap between the two arcs) and gs (bandwidth), respectively.

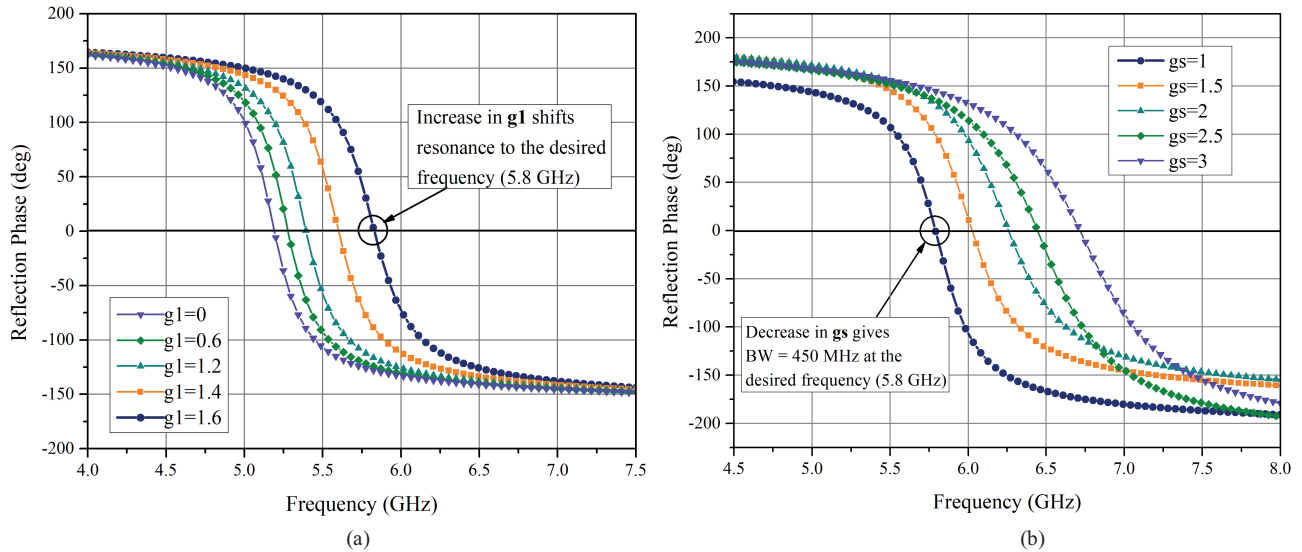


Figure 5. (a) Parametric analysis on $g1$ to study the resonance control mechanism. (b) Parametric analysis on gs to study the bandwidth effect.

In Figure 5a, a shift from 5.2 GHz to 5.8 GHz can be observed with the increasing value of $g1$, while precisely at $g1 = 1.6$ mm, the graph acquires the desired frequency of operation. On the other hand, as evident from Figure 5b, the value of gs drastically impacts the bandwidth. The thicker the arc, the better would be its bandwidth, all this at the cost of a significant shift from the desired operating band. Therefore, the value

of g_s is maintained at 1 mm to achieve the required frequency. After simultaneously adjusting the values of g_l and g_s , the 0° shift occurs exactly at 5.8 GHz with the acquired bandwidth of 450 MHz (5.5 GHz - 5.95 GHz) within the phase range of -90° to $+90^\circ$ [24].

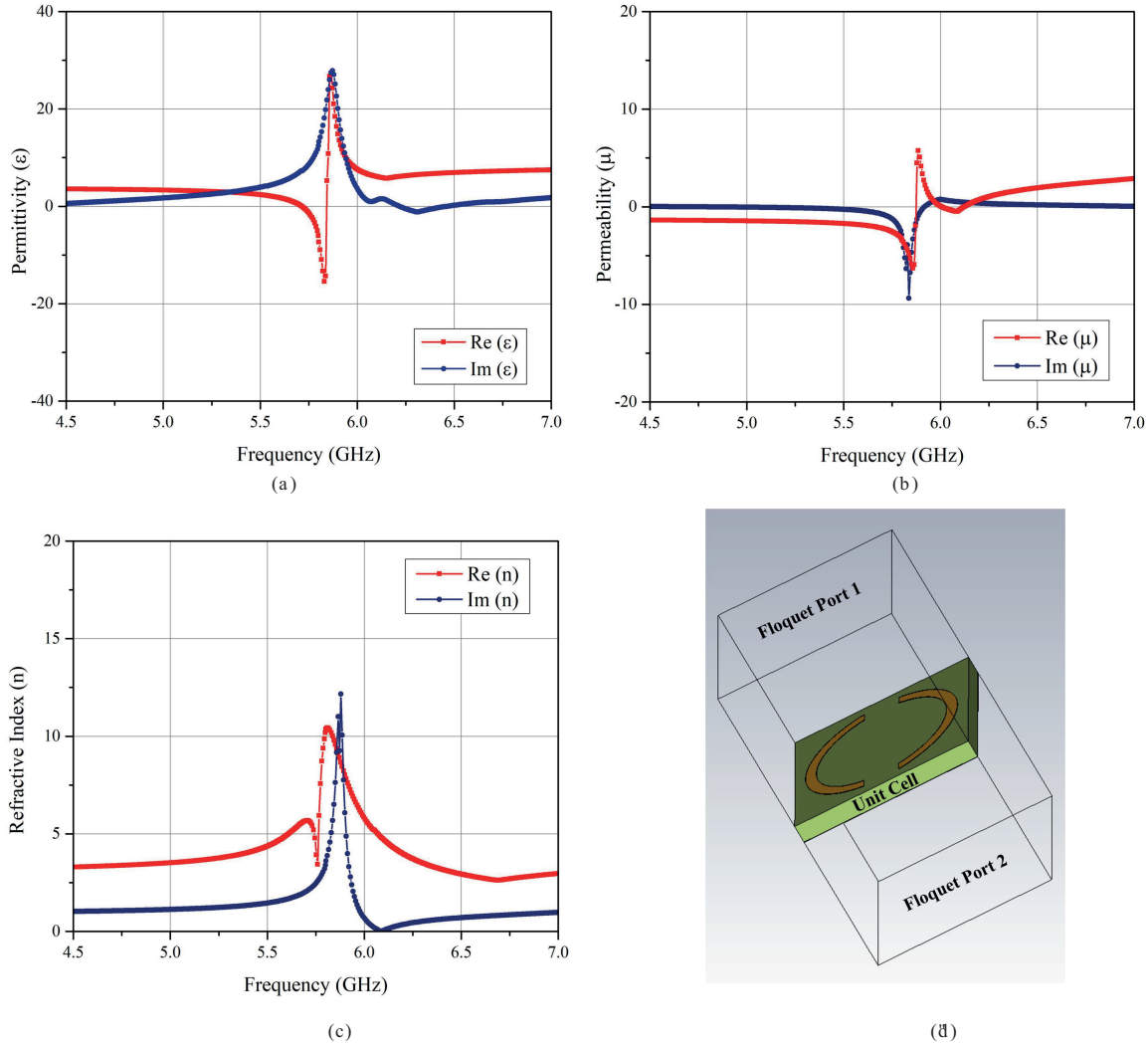


Figure 6. Retrieved material parameters of the proposed unit cell and analysis setup (a) permittivity, (b) permeability (c) refractive index, (d) simulation setup of the unit cell.

In addition, the metamaterial intrinsic characteristics such as permittivity, permeability, and refractive index are extracted from the scattering parameters (reflection and transmission coefficient) of the proposed unit cell structure. Both real and imaginary parts of the extracted permittivity, permeability, and refractive index are manifested in Figures 6a–6c, respectively. As evident, both the permittivity and permeability experience a transition in value from positive to negative exhibiting negative characteristics in the particular frequency region, which justifies its utility as a metamaterial structure, whereas the refractive index displays near-zero characteristics [33]. The simulation environment detailing the boundary conditions employed for analysis of the unit cell is manifested in Figure 6d.

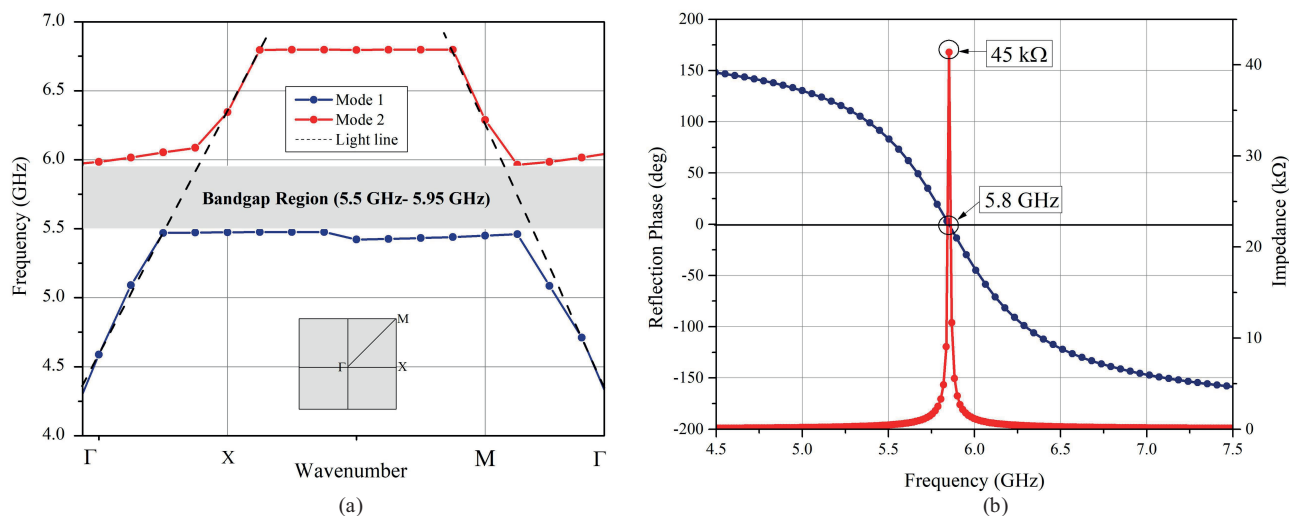


Figure 7. (a) EBG unit cell dispersion diagram. (b) EBG unit cell impedance performance.

Further, Figure 7a represents the dispersion diagram depicting bandgap region from 5.5 GHz to 5.95 GHz while Figure 7b outlines the impedance feature of the designed EBG unit cell where it retains high impedance of $45\text{k}\Omega$ at 5.8 GHz.

3. Integration of antenna with EBG

Further, if the initially designed antenna is placed directly on the body, the severity of the high dielectric tissues will degrade its radiation performance explicitly. Thereby, to minimize the effect of the human body on the antenna and to enhance its radiation characteristics, the antenna is combined with the EBG structure forming an array of 2×2 . The endeavor to reduce the overall lateral dimensions serves as the rationale behind retaining the EBG size to 2×2 . However, there exists a possibility to extend it to either 3×3 or 4×4 but as discernible from [3, 16], these high-profile structures transpired only marginal improvement in the peak gain comparative to the prime size while other antenna characteristics remain preserved with slight effect on the impedance.

As the antenna is backed by an EBG structure, the electromagnetic interference between the two may create discrepancies in terms of degraded radiation efficiency and impedance mismatch. Hence, an appropriate separation between the two structures is required to minimize coupling and maintain a good impedance match [13, 28]. Therefore, the antenna is positioned at approximately $0.029\lambda_0$ above the EBG structure, and a flexible foam is inserted to fill the space amid the antenna and EBG to prevent direct electrical contact that may cause short circuit [27]. This precise value has been set by carefully performing the simulations to observe the impact of variation in distance with the aim to yield desired impedance match with minimum coupling. Moreover, to account for the frequency detuning caused by the EBG, the antenna geometry is reoptimized according to the requirements to achieve the best results. For this purpose, after a deliberate analysis, the ground is repositioned at a marginal gap (Gp) and feed-line dimensions are readjusted which assisted in acquiring the desired impedance match. The overall dimensions of the integrated design measures approximately $32 \times 32\text{ mm}^2$ ($0.6\lambda_0 \times 0.6\lambda_0$). The fabricated prototype of the antenna is depicted in Figure 8.

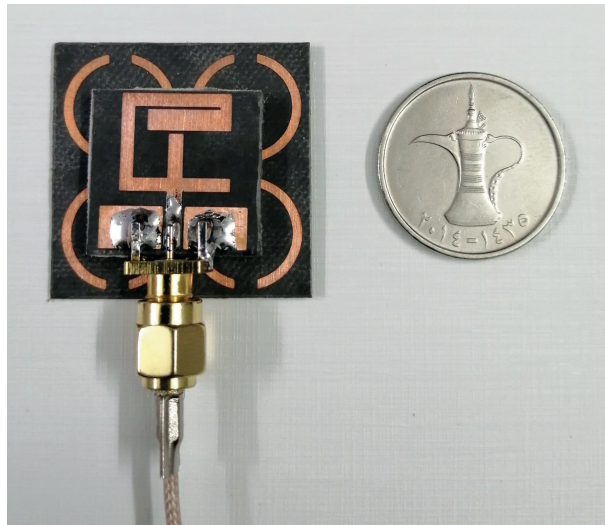


Figure 8. Fabricated illustration of the proposed EBG-backed antenna.

4. Results and discussion

4.1. Reflection coefficient

To assess the performance of the presented antenna model for all of its characteristics, namely reflection coefficient and radiation pattern, they were first examined by their simulation results and then through measurement.

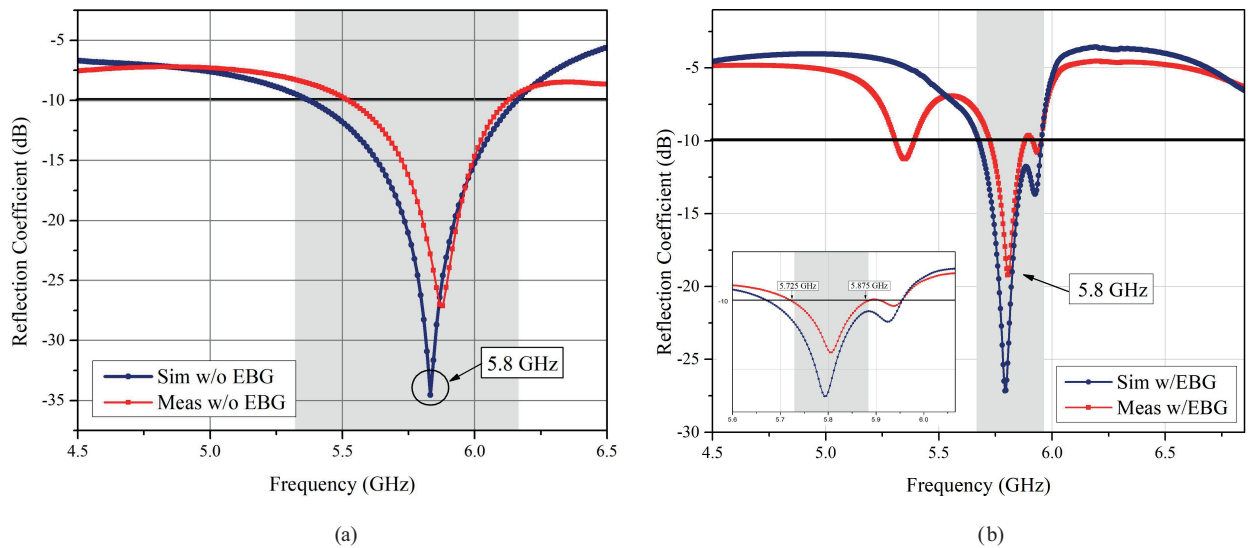


Figure 9. (a) Simulated and measured reflection coefficient of the antenna w/o EBG. (b) Simulated and measured reflection coefficient of the antenna with EBG.

Figures 9a and 9b present both the simulated and measured results of the antenna without and with EBG, respectively. As it can be seen, the measured results overlay the corresponding simulated results and are reasonably in accord with each other except that in case of antenna alone, a slight shift to a higher band is observed for the measured S_{11} while that of the antenna with EBG, the resonance experiences a negligible

frequency offset with slight contraction, but it covers the ISM band (5.725–5.875 GHz) with 4.3% impedance bandwidth. However, the bandwidth was slightly higher in the simulated outcome. The result aligns with [13]. The bandwidth to experience a slight degradation for its measured outcome signify the imprecision of the fabrication and measurement procedure.

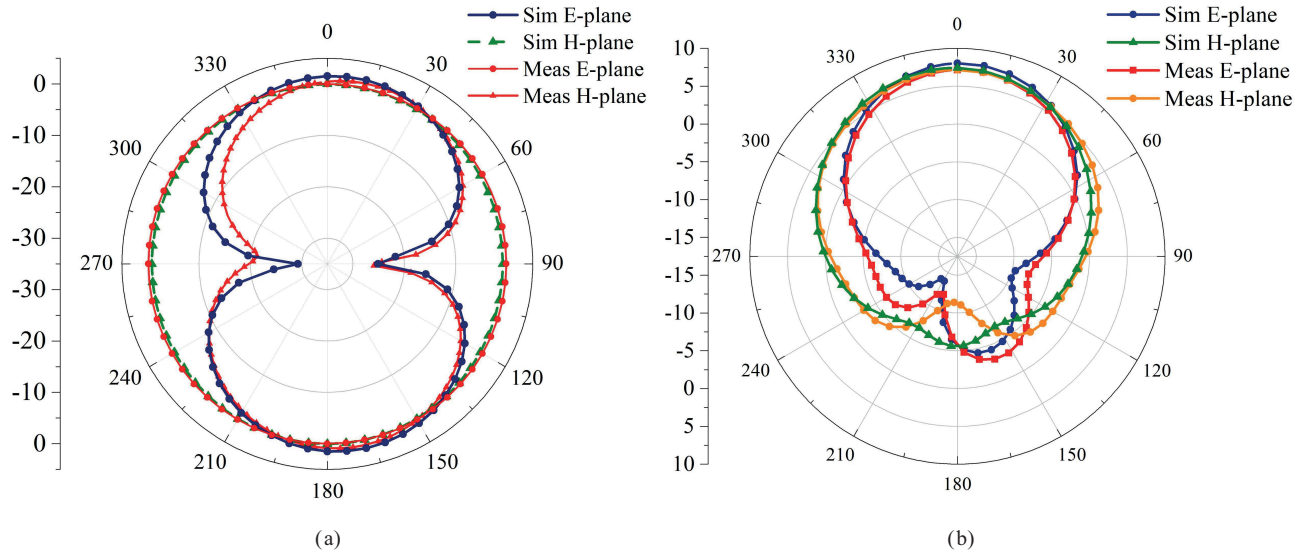


Figure 10. (a) Simulated and measured radiation pattern of the antenna in E and H-plane.(b) Simulated and measured radiation pattern of the EBG-backed antenna in E and H-plane.

4.2. Radiation pattern and gain

Another performance metric to be assessed is the radiation pattern of the antenna, which is displayed in Figure 10 for both the simulated and measured cases, respectively.

The antenna without EBG retains an omni-directional pattern in H-plane (xz-plane) and a dipole resembling pattern in E- plane (yz-plane) possessing high backward radiation. However, in the presence of EBG, the resulting pattern was directional in nature as clear from Figure 10b, which depicts how the integration of EBG reduces the impact of electromagnetic radiations. Not only a directive pattern is achieved, but the gain has been significantly improved for the integrated antenna reaching up to 7.2 dBi with increased front to back ratio falling in the range of 11–13 dB where initially, the gain was only 2.9 dBi for the basic antenna. The simulated gain and FBR of the integrated design is exhibited in Figure 11. The realized simulated efficiency for the antenna alone and with EBG is 95% and 85%, respectively. This slight degrade in efficiency can be accredited to the material losses encountered during integration.

5. On-body assessment

5.1. Structural conformability

To determine the antenna’s real-time suitability; user comfort and flexibility are major design considerations, more explicitly its operation when it is bent along a certain degree. Therefore, before proceeding to the on-body assessment, the antenna has been analyzed for its bent configuration performance to ensure structural consistency and robustness.

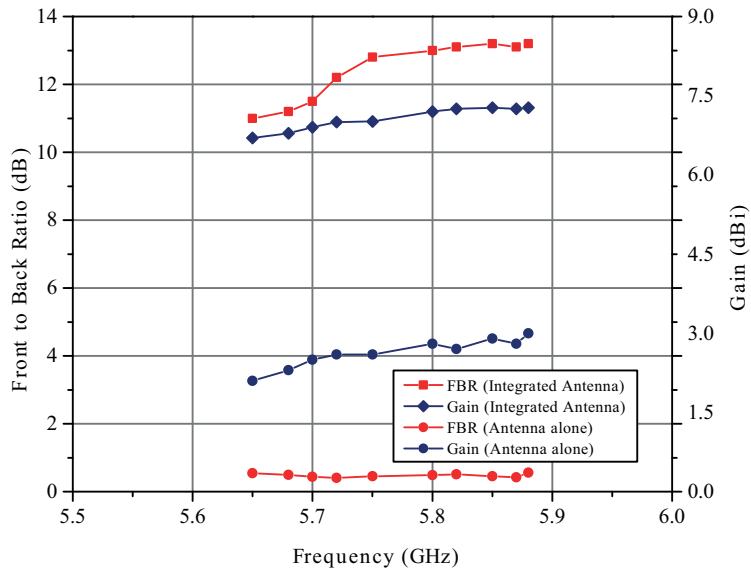
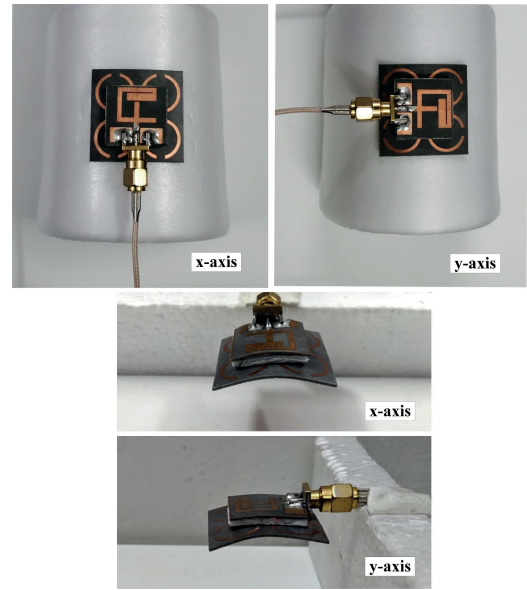
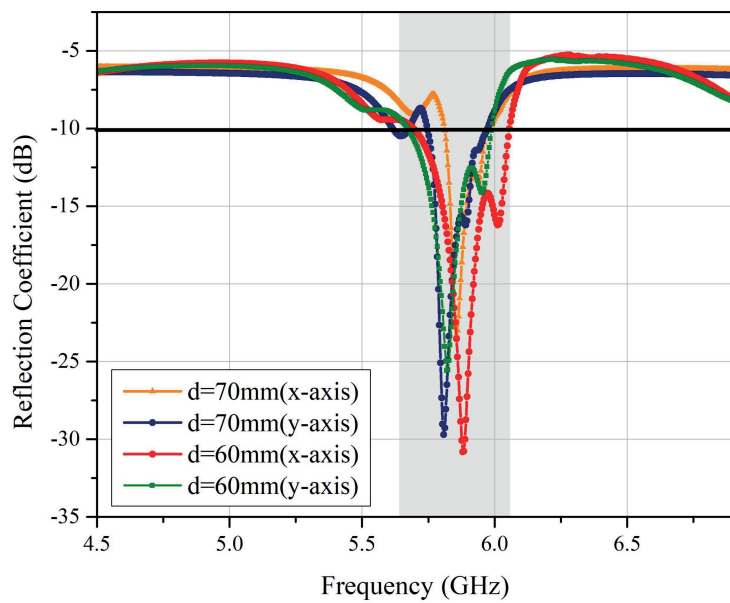


Figure 11. Simulated gain and front to back ratio.



(a)

(b)

Figure 12. (a) Measured reflection coefficient of the bent antenna for varied diameter configurations. (b) Bending along x-axis and y-axis.

For assessment, diameter comparable to the size of a leg and forearm have been deliberately chosen for bending evaluation which serves as the worst conformal configuration as well undergo extreme movement. To support the structural robustness claim, an experimental evaluation is carried out where the antenna is first bent over a cylinder, which is 60 mm in diameter, for both axes, namely x-axis and y-axis and then the diameter is increased to 70 mm. The antenna is cohered over the cylinder using an adhesive tape. The reflection coefficient

for the varied diameter configuration is shown in Figure 12a.

With the reduction in diameter along x-axis, a marginal shift to higher frequency is apparent while in view of y-axis, a slight decrease in the impedance of antenna can be observed. Ideally, the antenna's resonant frequency and radiation characteristics are to be retained regardless of the bent axis. From Figure 12, it can be inferred that the antenna resonant frequency suffered minor shift while still preserving the particular band of operation. This extremely small detuning can be attributed to a change in the current distribution with varied bend angles [13]. The measured gain of the bent antenna, along x and y-axis, when $d = 60$ mm and $d = 70$ mm remained in the range of 6.6 dBi and 6.9 dBi, respectively. As for efficiency, along both axes, in either variation of diameter stayed above 70%. Moreover, as the antenna is structurally compact, therefore, it remains conformal to the human body and suffers little deformation when placed on the body, which exhibits its operational consistency [14].

5.2. Human tissue loading evaluation

After the precise study of the antenna parameters in free space, the next step is its experimental evaluation in the presence of the human body to examine the possible impact of high permittivity tissues on the antenna's performance.

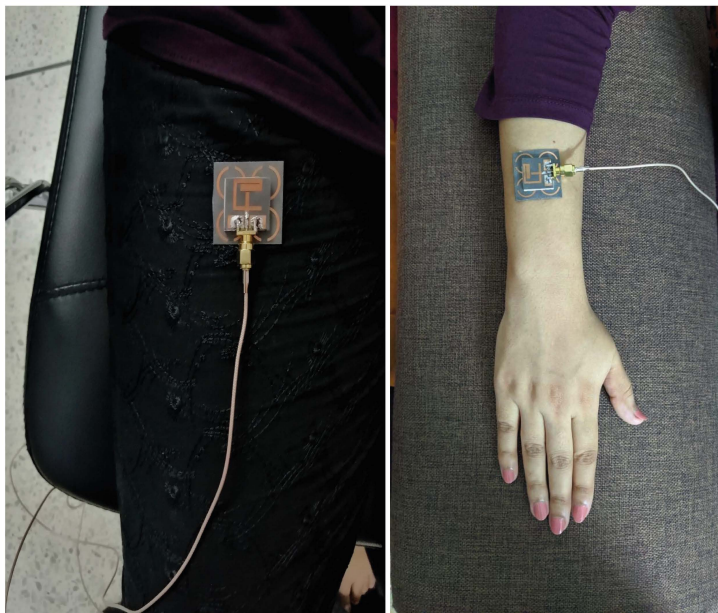


Figure 13. On-body assessment of the EBG-backed antenna.

For measured on-body results, the fabricated prototype has been assessed on the leg and arm of a female volunteer weighing 64 kg and height 163 cm as it can be seen in Figure 13.

When the antenna is placed directly on the human body, precisely on arm and leg, a shift in the resonance frequency to a lower band can be observed with slightly improved bandwidth. The minute widening in the bandwidth of the basic antenna is a consequence of degraded quality factor of the radiating element when loaded against the human body [13]. One of the main reasons is that the dielectric constant of the body is much higher than that of the substrate, dramatically creating a mismatch in the antenna's overall performance.

Besides, the dispersive nature of human tissues absorbs a significant amount of emitted electromagnetic radiation from the antenna.

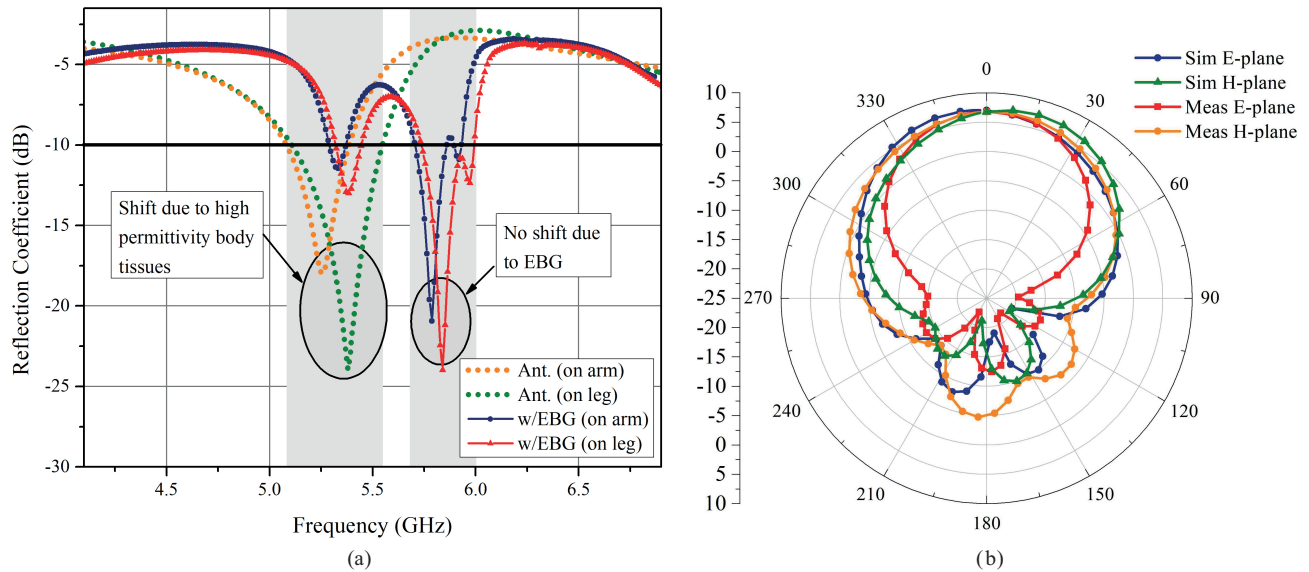


Figure 14. (a) Measured on-body reflection coefficient for the antenna alone and with EBG.(b) On-body radiation pattern of the EBG-backed antenna in E and H-plane.

Conversely, the antenna backed by EBG possesses a stable reflection coefficient $S_{11} < -10$ dB for the desired frequency while preserving all of the antenna parameters due to the high isolation caused by the EBG surface. Figure 14 illustrates the measured on-body reflection coefficient and radiation pattern. Clearly, the measured outcome is in unison with the simulated results.

Furthermore, in case of the antenna alone, the radiation pattern is greatly influenced by the dispersive nature of human tissues absorbing a significant amount of emitted electromagnetic radiation from the body. On the contrary, the integrated antenna retains almost the same pattern with slight anomalies with its FBR slightly improved because the body acts as an extension of the ground plane thereby, enlarging the total surface area which consequently directs the radiation away from the body. It can be inferred from the results shown in Figures 14a and 14b, that EBG provides considerable isolation meanwhile significantly enhances the radiation characteristics of the antenna. During on-body assessment of antenna performance, the gain on arm and leg constitutes to 6.6 dBi and 6.4 dBi, respectively and efficiency in that case is 79% and 77%, respectively.

6. Specific absorption rate (SAR)

One of the determining factors for the adequacy of a wearable device is the specific absorption rate (SAR), which governs the safety regulations for devices to be placed in proximity of the human body. SAR is a factor that signifies the amount of electromagnetic radiation absorbed in the body.

As per the regulatory bodies ICNIRP and FCC, the maximum SAR value must not be higher than 2 W/kg for 10g and 1.6 W/Kg for 1g of tissue, respectively [35]. To determine the SAR factor for the proposed design, a series of simulations were carried out on an artificially developed body phantom, whereas the calculations were performed as per the IEEE C95.1 standard available in CST MWS software while retaining the input power at 100 mW. It must be noted that any increase in reference power would consequently amplify the energy

absorption in the tissue. Considering the safety measures, it is advised not to excite the antenna beyond 100 mW input power in case of wearable devices [19]. Therefore, the designed antenna is deliberately tested at 100 mW to study its SAR performance at high power.

Table 1. Human tissue properties at 5.8 GHz.

Layer	Thickness (mm)	ϵ_r	Conductivity σ (S/m)	Density (kg/m ³)
Skin	2	35.114	3.717	1090
Fat	3	4.95	0.29313	930
Muscle	23	48.485	4.9615	1050

For SAR simulations, a multilayer cuboid of $90 \times 90 \times 35 \text{ mm}^3$ emulating the human body has been utilized, which comprises of three layers imitating the skin, fat and muscle. The thickness, permittivity, conductivity and density values of each of the layer are collated in Table 1.

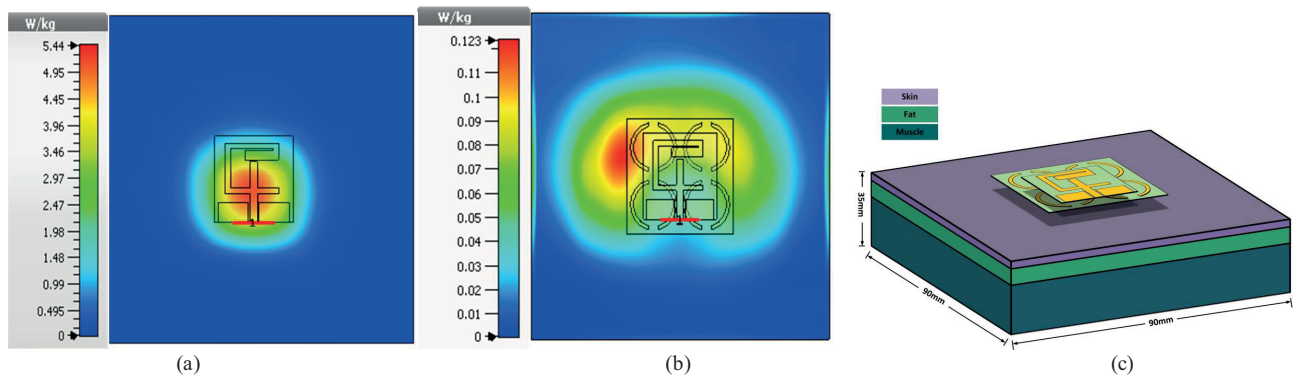


Figure 15. (a) SAR distribution of the basic antenna. (b) SAR investigation of the EBG-backed antenna. (c) Layered tissue phantom with the EBG-backed antenna.

Moreover, the separation between the antenna and modelled tissue is critical in performance assessment. In general, the gap substitutes for the fabric of wearer; thereby, for SAR calculations, it has been retained at the distance of 2 mm [27] as depicted in Figure 15c.

Table 2. SAR value of proposed antenna averaged over 1g and 10g tissue.

Input power	Averaged value	SAR w/o EBG (W/kg)	SAR with EBG (W/Kg)
100mW	1g	7.57	0.31
	10g	5.44	0.123

Figure 15 shows the SAR distribution of the modelled design of the basic antenna and the EBG backed antenna, averaged over 10g of biological tissue. Whereas, the Table 2 lists the SAR values obtained at 5.8 GHz for both 1g and 10g of the layered tissue model, respectively.

It can be inferred from the table that both the values of the EBG backed antenna are in accord, in fact, far less than the prescribed limitations from the regulatory bodies. Comparatively, the primary antenna gives high SAR value which exceeds the limit while EBG prominently reduces the SAR value up to 95%.

A comparative analysis of antenna parameters with the previously reported work have been compiled in Table 3. The analysis compares the performance metrics in terms of antenna dimensions, gain, FBR, utilized substrate and attained SAR value.

Table 3. Comparison of the previously reported wearables with presented design.

Ref.	Dimensions (λ_0)	Frequency (GHz)	No. of unit cell	Gain (dBi)	FBR (dB)	Reflected plane	Substrate	SAR(W/kg)	
								1g	10g
[3]	$1.01\lambda \times 1.01\lambda \times 0.05\lambda$	3.5/5.8	4×4	9.1/7.7	15	AMC	Rogers 3850	0.3	0.08
[6]	$2\lambda \times 1.33\lambda \times 0.07\lambda$	5.8	4×6	6.12	17	AMC	Pellon Fabric	0.61	1.18
[13]	$0.49\lambda \times 0.49\lambda \times 0.01\lambda$	2.45	2×2	6.55	13	EBG-FSS	Jeans	0.055	-
[14]	$0.59\lambda \times 0.59\lambda \times 0.04\lambda$	2.45/5.8	3×3	5.2/7.7	-	MTM	Polyimide	0.7	0.12
[16]	$0.47\lambda \times 0.70\lambda \times 0.05\lambda$	2.48	2×3	5.6	-	EBG	PDMS	0.05	-
[15]	$1.01\lambda \times 1.01\lambda \times 0.06\lambda$	2.45	4×4	8.55	12	AMC	Pellon Fabric	0.33	0.16
[17]	$0.66\lambda \times 0.66\lambda \times 0.03\lambda$	2.45	3×3	7.3	13	EBG	Felt	0.55	0.23
[28]	$0.73\lambda \times 0.73\lambda \times 0.04\lambda$	2.45/3.3	3×3	6.4/3	-	AMC	Rogers RO3003	0.29	-
[29]	$1.22\lambda \times 1.22\lambda \times 0.03\lambda$	1.8/2.45	3×3	-	15	EBG	Jeans	0.024	0.02
[30]	$0.98\lambda \times 0.98\lambda \times 0.03\lambda$	2.45/5.8	3×3	6.4/7	15	EBG	Felt	0.4	0.31
[31]	$0.8\lambda \times 0.8\lambda \times 0.03\lambda$	2.45/5	4×4	-	12	AMC	Felt	-	0.03
[33]	$1.51\lambda \times 1.51\lambda \times 0.07\lambda$	4.55-13	7×7	6	16-23.5	MTM	Felt	0.06	0.11
This work	$0.6\lambda \times 0.6\lambda \times 0.06\lambda$	5.8	2×2	7.2	13	EBG	RT/Duroid 5880	0.31	0.123

As apparent, the designed antennas in [3, 6, 15, 17] and [28]–[31] suffer from electrically large profiles with satisfactory performance. Moreover, in the research presented in [13]–[17], the targeted operational band is 2.45 GHz [27, 28], widely used for industrial, scientific and medical (ISM) band applications and thereby, undergo an increased interference due to being overoccupied with the working medical equipment [32]. Antennas operating at lower frequencies suffer from low bandwidth problem and large dimensions which leads to user discomfort when worn against body. The utilization of fabric substrate in [13, 15] and [29] is surely feasible but highly susceptible to crumpling under the dynamics of human body ensuing performance degradation, if exposed to moisture. In our executed work, a compact low-profile, robust and high-performance antenna for 5.8 GHz ISM applications is evaluated manifesting reduced lateral dimensions when paralleled against [15]–[33], higher gain than the research reported in [6, 16], comparable FBR with [13, 15], [28]–[31] and satisfies the ultimate low SAR requirement to support wearable applications which can be contrasted with the reported literature in [14, 17] and [30].

7. Conclusion

A conveniently compact, low-profile wearable antenna is detailed in this work. The design is scrutinized for its electromagnetic performance in both the free space and the on-body configuration for 5.8 GHz ISM applications. The target is to employ the antenna in telemedicine sector where antenna embedded wearable devices are required to remotely access the care facility. Deterioration in antenna performance in the wearable mode is mitigated by backing the design up by a novel EBG structure, providing desired isolation between the artifact and the human subject. Semiflexible characteristics and mechanical robustness associated with the chosen laminate solidifies the appropriateness of the proposed design for wearable applications. Integration of EBG

with the proposed antenna design has led to marked improvement in radiation characteristics concerning gain which escalated to 7.2 dBi and thereby alleviating the back radiation to improve the front to back ratio to 13 dB. Enhanced directivity and low SAR realization fulfil the requisite to serve as a wearable, making it a promising candidate for deployment in body-centric scenarios.

References

- [1] Ashyap AY, Dahlan SH, Abidin ZZ, Abbasi MI, Kamarudin MR et al. An overview of electromagnetic band-gap integrated wearable antennas. *IEEE Access* 2020; 8: 7641-58.
- [2] Ali SM, Sovuthy C, Imran MA, Socheatra S, Abbasi QH et al. Recent advances of wearable antennas in materials, fabrication methods, designs, and their applications: State-of-the-art. *Micromachines* 2020; 11 (10): 888.
- [3] El Atrash M, Abdalla MA, Elhennawy HM. A wearable dual-band low profile high gain low SAR antenna AMC-backed for WBAN applications. *IEEE Transactions on Antennas and Propagation* 2019; 67 (10): 6378-88.
- [4] Hall PS, Hao Y. *Antennas and propagation for body-centric wireless communications*. 2nd Ed. Norwood, MA, USA: Artech House, 2012.
- [5] Arif A, Zubair M, Ali M, Khan MU, Mehmood MQ. A compact, low-profile fractal antenna for wearable on-body WBAN applications. *IEEE Antennas and Wireless Propagation Letters* 2019; 18 (5): 981-5.
- [6] Alemaryeen A, Noghmanian S. On-body low-profile textile antenna with artificial magnetic conductor. *IEEE Transactions on Antennas and Propagation* 2019; 67 (6): 3649-56.
- [7] Ashyap AY, Abidin ZZ, Dahlan SH, Majid HA, Waddah AM et al. Inverted E-shaped wearable textile antenna for medical applications. *IEEE Access* 2018; 6: 35214-22.
- [8] Paracha KN, Rahim SK, Soh PJ, Kamarudin MR, Tan KG et al. A low profile, dual-band, dual polarized antenna for indoor/outdoor wearable application. *IEEE Access* 2019; 7: 33277-88.
- [9] Faisal F, Amin Y, Cho Y, Yoo H. Compact and flexible novel wideband flower-shaped CPW-fed antennas for high data wireless applications. *IEEE Transactions on Antennas and Propagation* 2019; 67 (6): 4184-8.
- [10] Farhat S, Arshad F, Amin Y, Loo J. Wideband patch array antenna using superstrate configuration for future 5G Applications. *Turkish Journal of Electrical Engineering & Computer Sciences* 2020; 28 (3): 1673-85.
- [11] Wagih M, Wei Y, Beeby S. Flexible 2.4 GHz node for body area networks with a compact high-gain planar antenna. *IEEE Antennas and Wireless Propagation Letters* 2018; 18 (1): 49-53.
- [12] Sambandam P, Kanagasabai M, Ramadoss S, Natarajan R, Alsath MG et al. Compact monopole antenna backed with fork-slotted EBG for wearable applications. *IEEE Antennas and Wireless Propagation Letters* 2019; 19 (2): 228-32.
- [13] Ashyap AY, Abidin ZZ, Dahlan SH, Majid HA, Kamarudin MR et al. Highly efficient wearable CPW antenna enabled by EBG-FSS structure for medical body area network applications. *IEEE Access* 2018; 6: 77529-41.
- [14] Wang M, Yang Z, Wu J, Bao J, Liu J et al. Investigation of SAR reduction using flexible antenna with metamaterial structure in wireless body area network. *IEEE Transactions on Antennas and Propagation* 2018; 66 (6): 3076-86.
- [15] Alemaryeen A, Noghmanian S. Crumpling effects and specific absorption rates of flexible AMC integrated antennas. *IET Microwaves, Antennas & Propagation* 2018; 12 (4): 627-35.
- [16] Gao G, Zhang R, Yang C, Meng H, Geng W et al. Microstrip monopole antenna with a novel UC-EBG for 2.4 GHz WBAN applications. *IET Microwaves, Antennas & Propagation* 2019; 13 (13): 2319-23.
- [17] Gao GP, Hu B, Wang SF, Yang C. Wearable circular ring slot antenna with EBG structure for wireless body area network. *IEEE Antennas and Wireless Propagation Letters* 2018; 17 (3): 434-7.
- [18] Corchia L, Monti G, Tarricone L. Wearable antennas: Nontextile versus fully textile solutions. *IEEE Antennas and Propagation Magazine* 2019; 61 (2): 71-83.

- [19] Azeez HI, Yang HC, Chen WS. Wearable triband E-shaped dipole antenna with low SAR for IoT applications. *Electronics* 2019; 8 (6): 665.
- [20] Hamouda Z, Wojkiewicz JL, Pud AA, Koné L, Bergheul S et al. Magnetodielectric nanocomposite polymer-based dual-band flexible antenna for wearable applications. *IEEE Transactions on Antennas and Propagation* 2018; 66 (7): 3271-7.
- [21] Gross FB. *Frontiers in Antennas: Next Generation Design Engineering*, New York, NY, USA: McGraw-Hill, 2011.
- [22] Ashyap AY, Zainal Abidin Z, Dahlan SH, Majid HA, Saleh G. Metamaterial inspired fabric antenna for wearable applications. *International Journal of RF and Microwave Computer-Aided Engineering* 2019; 29 (3): e21640.
- [23] Pei R, Leach MP, Lim EG, Wang Z, Song C et al. Wearable EBG-backed belt antenna for smart on-body applications. *IEEE Transactions on Industrial Informatics* 2020; 16 (11): 7177-89.
- [24] Yalduz H, Koç B, Kuzu L, Turkmen M. An ultra-wide band low-SAR flexible metasurface-enabled antenna for WBAN applications. *Applied Physics A* 2019; 125 (9): 1-1.
- [25] Yang F, Rahmat-Samii Y. *Electromagnetic band gap structures in antenna engineering*. Cambridge, UK: Cambridge university press; 2009.
- [26] Abbasi MA, Nikolaou SS, Antoniadis MA, Stevanović MN, Vryonides P. Compact EBG-backed planar monopole for BAN wearable applications. *IEEE Transactions on Antennas and Propagation* 2016; 65 (2): 453-63.
- [27] Ashyap AY, Abidin ZZ, Dahlan SH, Majid HA, Shah SM et al. Compact and low-profile textile EBG-based antenna for wearable medical applications. *IEEE Antennas and Wireless Propagation Letters* 2017; 16: 2550-3.
- [28] Saeed SM, Balanis CA, Birtcher CR, Durgun AC, Shaman HN. Wearable flexible reconfigurable antenna integrated with artificial magnetic conductor. *IEEE Antennas and Wireless Propagation Letters* 2017; 16: 2396-9.
- [29] Velan S, Sundarsingh EF, Kanagasabai M, Sarma AK, Raviteja C et al. Dual-band EBG integrated monopole antenna deploying fractal geometry for wearable applications. *IEEE antennas and wireless propagation letters* 2014; 14: 249-52.
- [30] Zhu S, Langley R. Dual-band wearable textile antenna on an EBG substrate. *IEEE transactions on Antennas and Propagation* 2009; 57 (4): 926-35.
- [31] Yan S, Soh PJ, Vandenbosch GA. Low-profile dual-band textile antenna with artificial magnetic conductor plane. *IEEE Transactions on Antennas and Propagation* 2014; 62 (12): 6487-90.
- [32] Li YJ, Lu ZY, Yang LS. CPW-fed slot antenna for medical wearable applications. *IEEE Access* 2019; 7: 42107-12.
- [33] Yalduz H, Tabaru TE, Kilic VT, Turkmen M. Design and analysis of low profile and low SAR full-textile UWB wearable antenna with metamaterial for WBAN applications. *AEU-International Journal of Electronics and Communications* 2020; 126: 153465.
- [34] CST Microwave Studio. [Online]. Available: <http://www.cst.com>
- [35] C95.1-2005 - IEEE Standard for Safety Levels with Respect to Human Exposure to Radio Frequency Electromagnetic Fields, 3 kHz to 300 GHz.